Applications in Engineering Science 7 (2021) 100056

Contents lists available at ScienceDirect

Applications in Engineering Science

journal homepage: www.elsevier.com/locate/apples

Interlocking mechanism design based on deep-learning methods

Marco Maurizi*, Chao Gao, Filippo Berto

NTNU - Norwegian University of Science and Technology, Department of Mechanical and Industrial Engineering, Trondheim 7491, Norway

ARTICLE INFO

Keywords:
Interlocking
Sutured lines
Machine learning
Mechanical properties

ABSTRACT

Biological structural systems such as plant seedcoats, beak of woodpeckers or ammonites shells are characterized by complex wavy and re-entrant interlocking features. This allows to mitigate large deformations and deflect or arrest cracks, providing remarkable mechanical performances, much higher than those of the constituent materials. Nature-inspired engineering interlocking joints has been recently proved to be an effective and novel design strategy. However, currently the design space of interlocking interfaces relies on relatively simple geometries, often built as a composition of symmetric circular or elliptical sutured lines. In the present contribution it is shown that deep-learning (DL) methods can be leveraged to enlarge the design space. Accurate and fast assessments of stiffness, strength and toughness of interlocking interfaces, generated through a cellular automaton-like method, can be obtained using a convolutional neural network trained on a limited number of finite element results. A simple application of a DL model for the recognition of interlocking mechanisms in 2-D interfaces is introduced. It is also shown that DL models, pre-trained on small resolution geometries, can accurately predict structural properties on larger design spaces with relatively small amounts of new training data. This work is addressed to give new insights into the study and design of a new generation of advanced and novel interlocked structures through data-driven methods.

1. Introduction

Millions of years of evolution have selected biological structures able to efficiently exploit the available resources whilst achieving high functional performance (Ortiz and Boyce, 2008; Wegst and Ashby, 2004; Wegst et al., 2015). Unique combinations of strength, stiffness, toughness, energy absorption and deformability emerge from specific hierarchical architectures and geometries, such as those observed in the tooth enamel (Bajaj et al., 2010), the bone (Koester et al., 2008), the nacre (Barthelat et al., 2007) or the turtle carapace (Krauss et al., 2009). Specifically, this latter, the beak of woodpeckers (Lee et al., 2014), and the human skull (Miura et al., 2009), represent examples of biological sutures, in which two mechanically interdigitated stiff skeletal components, i.e. hard building blocks, interlock together through a compliant soft interface, determining biological and mechanical functions, such as growth, respiration, locomotion and energy dissipation (Chen et al., 2015; Jaslow, 1990). Complex wavy geometries and re-entrant local features allow to mitigate the effect of large deformations via sliding and/or rotation of the constitutive building blocks (Gao et al., 2018; Mirkhalaf et al., 2018), dissipate energy through large volumes (Barthelat et al., 2016), and deflect or arrest cracks, enhancing fracture toughness (Liu et al., 2020). In particular, interlocking geometrical features are themselves able to improve the mechanical response of suture joints, increasing simultaneously strength, toughness and energy dissipation (Lin et al., 2014; Malik and Barthelat, 2018; Malik et al., 2017), and avoiding also catastrophic failure of inherent brittle base components, such as glass and ceramics (Mirkhalaf et al., 2016; 2018).

In the last decade research has been focused on the physical understanding and on the structure-property relationships of biological sutures and interlocked micro-structures (Fig. 1A), obtaining various analytical models (Gao and Li, 2019; Li et al., 2011; 2013; Malik et al., 2017) which can assess effective mechanical properties of simple geometries, such as triangular, rectangular, trapezoidal and anti-trapezoidal shapes. Pull-out response of symmetric and periodic jigsaw-like interlocked features has been studied via analytical and numerical modeling (Malik and Barthelat, 2018; Malik et al., 2017), demonstrating the relative contribution of geometry and friction coefficient on the pull-out strength and energy absorption. In addition, bi-stable interlocking and multi-locking geometries (Malik and Barthelat, 2018; Mirkhalaf and Barthelat, 2017) have highlighted the possibility to enrich the design space by adding other interlocking features, i.e., increasing the number of parameters necessary to define the geometry itself. Simultaneously, fractal-like interlocking architectures, occurring often in biological systems (Krauss et al., 2009; Li et al., 2012), have been observed to significantly enhance the effective mechanical performances (Khoshhesab and Li, 2018; Li et al., 2012; Wang et al., 2020), without adding other

* Corresponding author.
E-mail addresses: marco.maurizi@ntnu.no (M. Maurizi), chao.gao@ntnu.no (C. Gao), filippo.berto@ntnu.no (F. Berto).

https://doi.org/10.1016/j.apples.2021.100056
Received 11 March 2021; Received in revised form 15 March 2021; Accepted 18 May 2021
Available online 20 May 2021

geometrical parameters other than the fractal hierarchy. Stimulated from recent breakthroughs in machine learning (ML), specifically deep learning (DL) (LeCun et al., 2015), in this work the aim is to explore and enlarge new design spaces for structures based on the interlocking mechanism via a deep-learning approach, overcoming the limits of geometric simplicity and restricted number of parameters required from analytical models to assess the mechanical response as well as the impossibility to numerically simulate all the possible combinations in a specific design space. It is fundamental to emphasize that this approach may be extended to all engineered architectured material systems, for which geometric features and patterns are the main controllable engineering variables, as nature-inspired design, and more recently the lithomimetics (Beygelzimer et al., 2021), have shown to the scientific community. It is well known that it is impossible to mimic some aspects of natural structures transferring them to real man-made structures. For example, self-healing and regeneration mechanisms typical of bones can be only partially captured and reproduced in a real structure. However, geometrical aspects play a role which is not less important and they can be completely controlled with the advances of new design and manufacturing technologies. Fatigue failures, for example, are strongly affected by the local geometry of the structure, which is in many cases the most critical aspect. Taking therefore inspiration from natural structures (not completely mimicking them) can lead to new design opportunities that will be discussed in the present contribution.

Exploiting of the increase in the amount of computational power and available data, deep-learning techniques, and ML as a whole, have shown to dramatically improve the state-of-the-art of various fields, such as image and speech recognition, object detection, drug discovery and protein structure prediction (LeCun et al., 2015; Senior et al., 2020; Zhavoronkov et al., 2019). Since the early results on the universal approximation theorems, proving the capability of multilayer feedforward neural networks with just one hidden layer to approximate (under some measure) any function (in some domain) (Hornik, 1991; Lin and Jegelka, 2018), it has been known that machine-learning methods allow to approximate complex input-output functional relationships, detecting patterns in raw data given as input, through a learning process. Deep-learning computational models, specifically, are composed of successive layers, able to automatically discover intricate patterns and capture features with multiple levels of representation, directly from raw data (LeCun et al., 2015). Given, for example, an input $\mathbf{x}_i \in \mathbb{R}^n$, $1 \leqslant n < \infty$, representing some data i sampled from a probability distribution $P(\mathbf{x})$, and associated labels $\mathbf{y}_i \in \mathbb{R}^d$, $1 \leqslant d < \infty$, a deep-learning model is able to infer either the conditional $P(\mathbf{y} \mid \mathbf{x})$, $P(\mathbf{x} \mid \mathbf{y})$, or the joint $P(\mathbf{x}, \mathbf{y})$ probability distribution, depending on the specific model (Alpaydin, 2020).

Successful applications of DL in the fields of mechanics of solids, materials science and materials design have demonstrated its potentialities in the characterization of microstructures, prediction of material properties and inverse design problem (Bock et al., 2019; Chen and Gu, 2020); it is worth mentioning just few significative examples. Zijiang Yang et al. implemented deep-learning models, linking the composite material microstructure to its macroscopic effective stiffness (Yang et al., 2018). Charles Yang et al. proved the ability of convolutional neural networks (CNN) to accurately predict the stress-strain curves and the mechanical properties of two-dimensional binary composite materials, reducing the problem complexity through principal component analysis (PCA) (Yang et al., 2019; 2020). Along this path, Grace X. Gu et al. proposed new DL-based approaches for the design of hierarchical and binary composite systems (Gu et al., 2018a; 2018b), showing the capabilities of CNNs to classify and rank geometric designs, based only on limited information, such as "good" or "bad" design variables. Despite various reports of DL methods for studying composite materials can be found, to the best of our knowledge, the interlocking mechanism has never been studied in a DL-based framework.

In this work, we study the 2-D topological interlocking mechanism between two solid phases i.e., two separated parts, discretized through building blocks (Fig. 2), by designing a DL algorithm, able to accurately and rapidly predict the effective stiffness (E), strength (σ) and toughness (Γ), hence, providing a powerful tool to enlarging the design space of 2-D interlocked features. In Fig. 1 the basic idea behind this work is underlined. Starting from the observation of how some biological systems (e.g. the exoskeleton of the *Phloeodes diabolicus* (Rivera et al., 2020)) have evolved peculiar (interlocking) features, our DL model is designed to generalize the structure-property relationships (mechanical properties in this case) in any interlocking interface. We also report how a DL approach can easily unveil the interlocking mechanism along any arbitrary direction in the simple case of a single interface between two phases by means of the effective stiffness value, being this latter ~ 0 in case of "unlocked" structure, or > 0 in case of interlocked structure. In addition, the ability of the DL models to make generalizations from limited data is demonstrated by predicting mechanical properties of and classifying interlocked geometries sampled from larger design spaces i.e., higher resolution in the geometry generation method (details in the Methods section), despite having the models been trained mainly on smaller resolution architectures. Thus, we prove that DL models can learn additional patterns from larger design spaces, "remembering" from previous training on smaller geometry resolutions, in a transfer-learning fashion.

2. Methods

2.1. Geometry generation

To generate 2-D interlocked configurations systematically under finite $M \times N$ design space, a cellular automaton-like method is developed as shown in Fig. 2. The design space is composed by two phases (black and grey phase shown in Fig. 2A-B). Each phase is generated by arranging building blocks in a M by N grid (Fig. 2B), represented by a matrix. A single building block can assume the value either 0 or 1, corresponding to the black and grey phase, respectively. In analogy to cellular automata models of biological systems, the generation of interlocked configurations is based on growth rules (see Supporting Information and Fig. A.1). However, the rules are not applied simultaneously in the whole grid, rather, a decision is made element-by-element, sequentially in each row. In Fig. 2A a sequence of steps during a geometry generation is shown. Starting from the base configuration, in which the black phase covers only the first row, a permutation of the second row by black cells is performed. From this point, the growth rules are sequentially enforced to each subsequent row. The resulting configurations can be interpreted as a gradual growth of the black phase towards the grey one.

In addition to the application of growth rules, the generation of interlocking systems needs also to meet the following constraints: (i) local and (ii) global constraints. (i) Since only two phases are required, the *path continuity* constraint is imposed, indicating that for each two building blocks in the same state (0 or 1), arbitrarily taken, it must be possible to reach one of them by tracing a continuous path, starting from the other one. Note that the admissible paths are only those constituted of vertical and horizontal segments, thus moving from one building block to its diagonal neighbors is not allowed. Examples of clusters i.e., cases of path continuity violation, are shown in Supporting Information Fig. A.1. Every geometry is also verified for *topological interlocking* at the building block level. For each column, the number of interfaces between the black and grey building blocks is determined. A minimum of three interfaces along one column (i.e., along the loading direction) guarantees interlocking. (ii) Volume fraction i.e., the volume of one of the two phases with respect to the total volume, f_1 and $f_2 = (1 - f_1)$, is controlled during the generation process. To reduce the number of possible combinations, a constant volume fraction, $f_1 = f_2 = 0.5$, is imposed for all the generated structures.

Three geometrical parameters are also employed to characterize the generated interlocking systems: *interlocking area*, *total contact area*, and *lobeyness* (Fig. 2E). The interlocking area is defined as the area of the

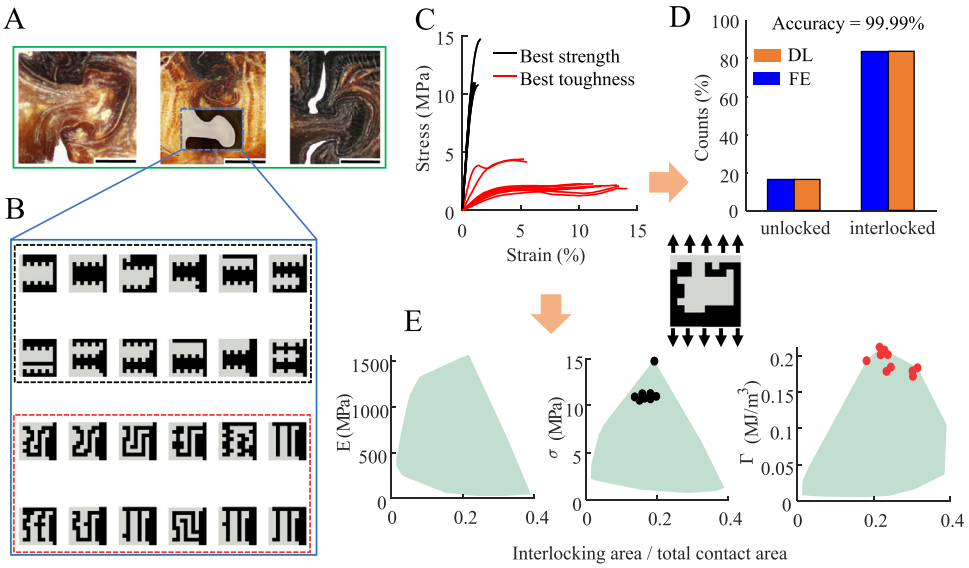

Fig. 1. Overview of the approach adopted in this work, starting from observation of biological systems naturally evolved, up to generating more complex interlocking features by a cellular automaton-like method, classifying them and predicting their mechanical properties through DL methods. **(A)** Characteristic interlocking features in the medial suture of some beetles: *A.verrucosus*, *P.diabolicus*, and *E.grandicollis*, from left to right, respectively (adapted from (Rivera et al., 2020)). Scale bar 100 μm. **(B)** Top 12 high- strength and toughness interlocking geometries in the top and bottom box, respectively, generated by the cellular automaton-like algorithm. The structures are sorted along the columns in descending order, for each row. **(C)** Stress-strain curves corresponding to the geometries in **(B)**. **(D)** Interlocking classification results from the DL model compared to the FE-based ground truth for a training data density of ~ 20%. **(E)** Large design space for stiffness, strength and toughness. The circles in the plots represent the mechanical properties computed from the curves shown in **C**. Geometries from the 10 by 10 system.

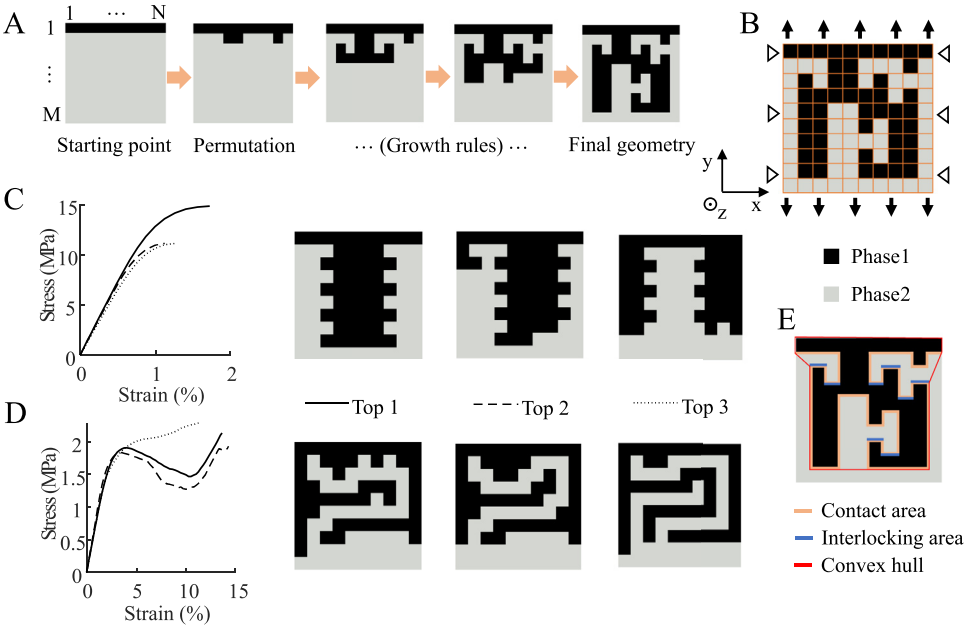

Fig. 2. **(A)** A sequence of generation of an interlocking feature by our cellular automaton-like method. **(B)** Building blocks composing an interlocking structure and boundary conditions of the FE model. Each building block is in turn discretized in the FE model, in which the uniform mesh size is 1/4 of the single block size, assumed to be unitary. Grey and black represent the distinct interlocking parts. **(C)** Top 3 high-strength geometries and corresponding stress-strain curves. Note that the second best geometry in the top box of Fig. 1B is not considered in the top 3 rank since it has same properties, being the complementary version of the best one. **(D)** Top 3 high-toughness geometries and corresponding stress-strain curves. **(E)** Definition of the geometric parameters considered in this work. Geometries from the 10 by 10 system.

interlocked surfaces (i.e., transmitting load). The total contact area is identified by the all area in contact between the black and grey phase. The lobeyness is a parameter borrowed from (Sapala et al., 2018), defined as the ratio between the perimeter of the boundaries of one phase and the length of its convex hull. Note that in the context of 2-D structures, the area of interfaces is equivalent to their length except for a rescaling factor (i.e., the out-of-plane thickness). Being such parameters unconstrained during data generation, they are considered as our geometric design variables. Nevertheless, they do not uniquely identify a geometry (Fig. 1E), proving the need to use DL methods to discover structure-property relationships.

To generate all the possible combinations of 2-D interlocking configurations in a finite design space a brute-force algorithm is adopted; the details of the algorithm are explained in Supporting Information and a flow-chart is shown in Fig. A.2. For a $M \times N$ design space, the possible combinations arise from the 2^{12} growth rules (Supporting Information Fig A.1), the 2^N permutations of the second row, and the imposed constraints ((i) and (ii) previously described). In this work, all the combinations are computed only for the 10 by 10 system. For higher resolutions, to limit the computational cost, a fixed number of random permutations of the second row is instead chosen.

2.2. Database generation

To generate a data set for training and testing the DL model for mechanical properties prediction under finite 10×10 design space, 18,594 interlocked configurations were generated by using the cellular automaton-like method. Removing the *interlocking* constraint, 19,946 geometries (including also the previous 18,594 interlocked configurations) were generated from the same design space, for training and testing the DL model for interlocking classification (i.e., identification of interlocked and unlocked geometries). In addition, 2,991 interlocked and 2,964 unlocked higher resolution geometries were generated from the 20 by 20 system with 100 random permutations of the second row

with and without the interlocking constraint, respectively. They constitute the data set used for training and testing the pre-trained (on 10 by 10 configurations) models by transfer learning.

2.3. Finite element model

To simulate highly nonlinear interlocking phenomena together with crack initiation and growth, 3-D finite element (FE) models were built by using the commercial FE software Abaqus 2017 (Abaqus/Explicit solver). Due to the different size of the required geometrical configurations, the dimensions of the FE model were 10 mm by 10 mm and 20 mm by 20 mm for the 10 by 10 and 20 by 20 system, respectively (Fig. 2B). The out-of-plane thickness is set to 0.25 mm for both cases. Eight-node brick elements (C3D8R) with reduced integration and a mesh size of 0.25 mm were used in the simulations. We also adopted a continuum elastic-perfectly plastic J2 model together with the definition of damage initiation and evolution (linear) to model the elasticity, initial yielding, plastic flow, and damage initiation and evolution of the base material (Young's modulus 4 GPa, Poisson's ratio 0.3, yield strength 30 MPa, fracture plastic strain 1%, plastic displacement at failure 0.05 mm). We assumed same material and damage properties for the two interlocking phases since only geometry effects were investigated. To model the contact of interlocking structures, a Coloumb friction model via the penalty contact method was used. The friction coefficient was set to 0.1. Displacement controlled boundary conditions were applied on interlocking structures as depicted in Fig. 2B. Specifically, the bottom face was constrained along the y-direction while the displacement along the y-direction was applied on the top face to achieve an effective maximum strain of 15%. The left and right faces were constrained along the x-direction. In addition, the out-of-plane displacements (z-direction) were constrained.

We obtained the mechanical behavior of the 2-D interlocking structures from the FE simulations and extracted the effective stiffness, strength and toughness from the stress-strain curves. The effective in-plane unidirectional stress and strain, indicated simply as stress and strain, were defined as the corresponding average values along the loading direction. Here, the stiffness was defined as the slope of the stress-strain curve at 0.01% of strain, the strength as the peak stress, and the toughness as the area underneath the curve. FE results are here considered as the ground truth when comparing them to the DL outcomes.

2.4. Deep-learning methods

The DL models used in this work are implemented in the machine-learning framework TensorFlow (Abadi et al., 2016). Two fundamental tasks are performed by the DL models: interlocking classification and mechanical properties prediction. For DL computations the geometry systems are represented by binary images, corresponding to the input of our DL models. The pixel resolution can be either equal to the system size (e.g. to a 10 by 10 geometry corresponds a 10 by 10 binary matrix) or resized to higher resolutions by a scale factor (e.g. to a 10 by 10 geometry could correspond a 20 by 20 binary matrix). Image resize is applied when the DL models are mainly pre-trained on smaller resolution geometries (10 by 10), and other data from larger design spaces (e.g. 20 by 20) are provided to the model for further training. The DL models implemented in this work are convolutional neural networks (LeCun et al., 2015), whose basic architecture is schematically shown in Fig. 3B.

2.4.1. Interlocking classification model

This model has a binary output, 0 or 1, for unlocked or interlocked geometry, respectively. Based on the stiffness value obtained by the FE model, a binary label (ground truth) is correspondingly associated to each image (geometry). Three convolutional blocks form the central part of the neural network after the input layer. Each block contains one convolutional layer, which consists of 32 filters computed using 3 by 3 patches, with unitary stride, and ReLu activation function. To regularize the training process and to reduce the problem dimensionality exploiting of the translation-invariance property of convolutional networks (Kauderer-Abrams, 2017), a batch normalization and a 2 by 2 average pooling layer are subsequently stacked after the first convolutional layer. The second block includes only a convolutional layer, in which zero padding is also performed. The last convolutional layer is followed by a batch normalization, whose output is then flattened into a vector. A fully-connected layer, with 64 neurons and Relu activation function, is next linked to the final classification layer, in which a sigmoid activation function maps the value into the range [0,1], representing in our case the probability of the input geometry being interlocked. The network is stochastically trained using Adam optimizer (a stochastic gradient descent method) for minimizing a binary cross-entropy loss function, with learning rate of 0.01 and batch size of 64. To avoid overfitting, early stopping regularization technique is implemented: the training process is stopped after 10 epochs in which the validation loss function does not decrease anymore, and the best network's weights are considered. We randomly split the 19,946 combinations of the 10 by 10 system into varying proportions of training, validation and test data. The influence of the training data density, varying from about 0.5 to 80%, was investigated (Supporting Information Fig. A.7A). Validation and test data densities were consequently equally split from the remaining data. Accuracy, precision and recall are used as metrics for performance evaluation, in which 0.5 is assumed as the threshold in the probability output for binary classification. Here accuracy is the fraction of predictions which match the ground-truth labels. Indicating with *positive* and *negative*, interlocking and unlocking classification, respectively, precision (PR) is defined by Eq. (1):

$$PR = \frac{TP}{TP + FP} \tag{1}$$

where TP and FP represent the number of true and false positives, respectively. Thus, it quantifies in our context the fraction of correctly identified interlocked geometries with respect to all the positive predictions. Recall (RE) is defined by (2):

$$RE = \frac{TP}{TP + FN} \tag{2}$$

where FN are the false negatives. RE measures the ability of the DL model to correctly classify actual interlocking geometries. Due to the simplicity of the single contact interface interlocking classification, tuning of hyperparameters, such as number and type of hidden layers, and number of filters, patch and stride size for convolutional layers, was not performed.

2.4.2. Mechanical properties regression model

The second DL model outputs three scalar values, which correspond to the stiffness, strength and toughness of the input geometry (Fig. 3B). Due to the different scales and probability distributions, as pre-processing step, the mechanical property values (from FE model) are normalized into the range $0 - 1$, subtracting the corresponding minimum value and dividing by the corresponding range of variation i.e., the difference between the greatest and the lowest property value. The DL output values are then inversely rescaled to obtain the original physical units. Stochastic training using Adam optimizer is adopted to minimize a mean squared error (MSE) loss function (between predicted and FE values), with learning rate of 0.01 and batch size of 64. As for interlocking classification, early stopping regularization technique is adopted. Only interlocking combinations were included in the data set for the 10 by 10 system (18,594 geometries). To increase the performances of the DL model, the training data are augmented (by a factor of 4) by rotating the geometries (images) of 180° and reflecting them with respect to the two orthogonal in-plane directions (x- and y-direction). Other rotations and reflections are not considered, to keep the information of loading direction unchanged. As for the interlocking classification model, the influence of training data density was investigated (Supporting Information Fig. A.7B) with the same proportions. Next to the MSE, other

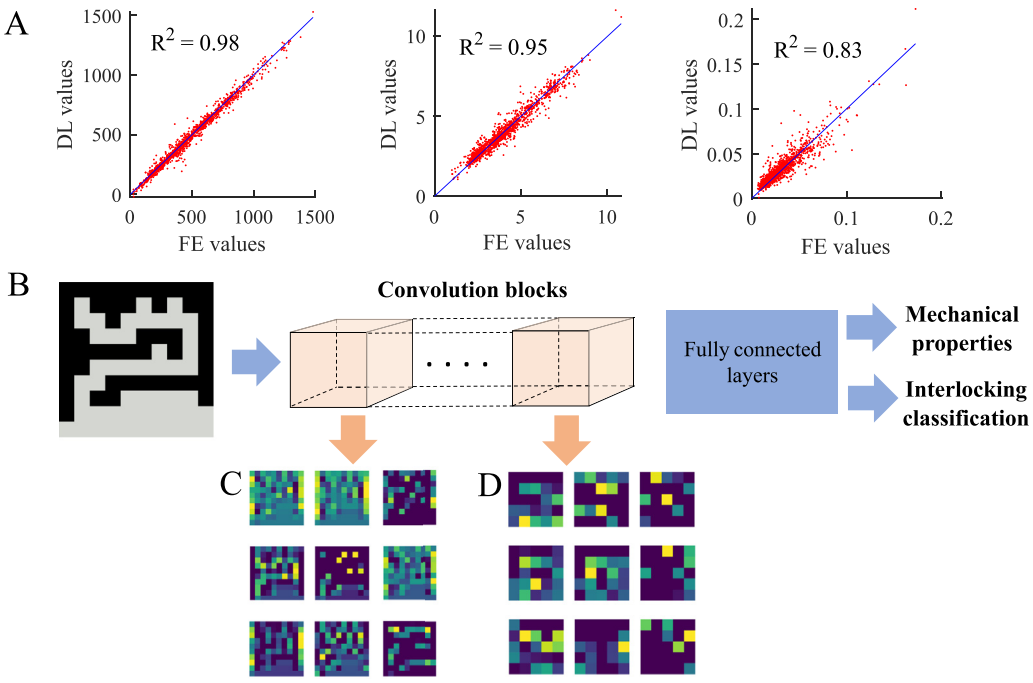

Fig. 3. **(A)** DL model predictions in order, for stiffness, strength and toughness, respectively, on test data (85:15 training-(validation-test) split). **(B)** Basic conceptual architecture of our DL models. **(C)** Visualization of 9 filters from the first convolutional layer of the DL model for mechanical properties prediction, corresponding to the best-toughness interlocking structure. **(D)** Analogous filters as in **C**, but from the second convolutional layer. Geometries from the 10 by 10 system.

metrics are considered for performance evaluation: the mean absolute error (MAE), which has the same unit of measure of the corresponding mechanical property, the relative MAE, which is the ratio between the MAE and the target property range, and the coefficient of determination (R^2) i.e., the squared of the Pearson coefficient. In addition, we define a prediction accuracy by Eq. (3):

$$\frac{\sum_{j=1}^{N_{td}} \{j \ : \ |\hat{y}_j - y_j| < k \left(\max_j(y_j) - \min_j(y_j)\right)\}}{N_{td}} \tag{3}$$

which quantifies the fraction of number of predictions $\hat{y}_j$ whose absolute distance from the target values y_j does not exceed a percentage $k \times 100$ of the target property range $\left(\max_j(y_j) - \min_j(y_j)\right)$. N_{td} indicates the total number of test data. k determines the arbitrary accepted error. We provide prediction accuracy values for $k = 0.05$ and 0.1. All the metrics are computed by averaging the results of 15 trials (with 95% confidence level), if not otherwise stated. To investigate possible high-performing network architectures on the 10 by 10 system, tuning of some hyperparameters (i.e., parameters of a DL model that govern the learning process without being updated during training) was performed. 24 different architectures were examined (Supporting Information Fig. A.5). Each model was characterized by a sequence of convolutional blocks, a flatten layer, and a fully connected layer with 256 neurons. A convolutional block was in turn composed of a 2-D convolutional layer, a batch normalization, and a 2 by 2 average pooling layer. The hyperparameters to be varied were the number of convolutional blocks (c), the number of filters (f), and the patch size (p) in each convolutional layer. 24 combinations of models arise from considering $c = 1, 2, 3$, $f = 8, 32, 64$, and $p = (3, 3), (5, 5)$, excluding the combination with $c = 1$ and $p = (5, 5)$, for each f. The number of convolutional filters was limited up to 64 to balancing computational costs and accuracy during the tuning process, in which relative increments in performances are important. The best 2 models among the 24 architectures were chosen evaluating MAE, R^2 and prediction accuracy (for $k = 0.05$). Note that the same data set was used for the evaluation of each model, setting the training data density to 85% and the validation and test data to 7.5% each. A further optimization was performed between the resulting 2 best models, whose performances were evaluated for $f = 64$ and 128 (Supporting Information Fig. A.6), leading to one optimized model.

2.4.3. *Transfer-learning approach*

To evaluate the capabilities of the DL models to make predictions on larger design spaces, a transfer-learning approach was furthermore adopted both for interlocking classification and mechanical properties prediction: geometries from the 20 by 20 system were fed into the pretrained (on the data set from the 10 by 10 system) network for further training in varying proportion, from 0.5% to 70% with a step of 5%, and from 0.5% to 80% with a step of 10%, for classification and properties prediction, respectively. The data set was composed of 2,991 interlocked and 2,964 unlocked configurations; the regression model was trained only with interlocked geometries. Metrics variations were consequently evaluated for each training data density.

3. Results

Analytical models allow to have a clear and powerful representation of materials' behavior and properties, however, only relatively simple geometries can be studied. Numerical physics-based models, such as FE modeling, can instead overcome such issue, at the cost of introducing computational limitations when dealing with large design spaces. Here we show how DL methods can tackle these problems, helping to accurately and rapidly recognize interlocking mechanism and predict mechanical properties of 2-D interlocking interfaces.

3.1. *Enlarging the design space*

To enlarge the design space of 2-D interlocking interfaces/joints, a cellular automaton-like method (described in Methods section and Supporting Information Fig. A.1 and A.2) was implemented. Stiffness, strength and toughness, solved by FE modeling, of all the combinations of the 10 by 10 system are plotted against the fraction of interlocking area with respect to the total contact area of the interface in Fig. 1E; the shaded area represents the maximum design space area covered by the

Table 1
Performances of the optimized DL model for mechanical properties prediction for the 10 by 10 system over 15 trials with a 85:15 train-(validation-test) split. The scores' mean values are provided together with their corresponding 95% confidence intervals. $Accuracy_5$ and $accuracy_{10}$ correspond to the accuracy computed with $k = 0.05$ and $k = 0.10$, respectively, from Eq. (3).

	MSE	MAE	Relative MAE (%)	R^2	$Accuracy_5$ (%)	$Accuracy_{10}$ (%)
Stiffness (MPa)	654.6 ± 71.38	17.43 ± 1.039	1.130 ± 0.0674	0.9899 ± 0.0010	98.17 ± 0.2558	99.78 ± 0.0742
Strength (MPa)	0.07487 ± 0.005409	0.1869 ± 0.007366	1.328 ± 0.0523	0.9684 ± 0.0019	93.88 ± 0.9569	99.02 ± 0.1919
Toughness (MJ/m^3)	$(64.03 \pm 6.784) \times 10^{-6}$	$(4.298 \pm 0.1) \times 10^{-3}$	2.088 ± 0.0486	0.8315 ± 0.0160	88.35 ± 1.496	96.77 ± 0.5750

mechanical properties for the specific geometry resolution. It is worth noting that the highest mechanical property values are reached for a geometric ratio of ~ 0.2, instead of the maximum value (~ 0.4) as intuitively expected. To investigate the possible correlations, the mechanical properties are also plotted one against each other, as shown in Supporting Information Fig. A.4A. A correlation ($R^2 = 0.66$) is found for strength and stiffness. Additionally, the three geometric parameters adopted to describe the geometries are also found to be partially correlated (Supporting Information Fig. A.4B). Specifically, lobeyness has a coefficient of determination $R^2 = 0.93$ with respect to the contact area, leading to the fact that only two out of three geometric parameters are statistically "independent". The other two combinations of parameters show only upper and lower bounds. The top 12 geometries for exhibiting the highest strength and toughness (from FE modeling) are shown in Fig. 1B in the upper and lower box, respectively. The corresponding stress-strain curves are displayed in Fig. 1C. It is clear that two distinct classes of geometries appear from the cellular automaton-like generation method for the 10 by 10 system: the geometries performing better in terms of strength or toughness show similar corresponding patterns for the two phases. Small and distributed interlocking surfaces generate higher strength due to a local compression loading transmission between the two solids. Instead, geometries exhibiting the highest toughness transmit load via local bending, allowing for larger deformations and strains. With similar patterns to the high-strength interlocking configurations, the top 12 high-stiffness geometries are shown in Supporting Information Fig. A.8. In Fig. 2C-D we report the best 3 geometries for the two classes (from FE modeling), highlighting the corresponding stress-strain curves. We want to specify that the inverted geometries (first two architectures in Fig. 1B) i.e., black and grey phases are inverted, obtained automatically from the algorithm, have same effective properties (under the assumption of identical base material). It is interesting to observe how high-strength geometries display a smaller nonlinear/plastic part than the high-toughness ones, which, in some cases, exhibit both softening and hardening before failure (top 1 and 2 in Fig. 2D). Therefore, the maze-like pattern of high-toughness geometries makes possible the local bending loading transmission, determining larger nonlinear/plastic regions, while the tree-like shape of high-strength interfaces promotes the local compression transmission mechanism, inducing a brittle-like behavior. A large design space is thus possible by implementing a cellular automaton-like approach. However, trade-off limitations between strength and toughness appear to be crucial for further optimization studies, which are beyond the scope of this work.

3.2. Interlocking classification

Nature exploits of the resources it has at hand, organizing them in a favorable way for better performances, which allow them to survive. Topological interlocking is one of the mechanisms of loading transmission between different solid constituents that have arisen from natural selection, allowing for high-performing designs (see for example Rivera et al., 2020 in Fig. 1A). To investigate how DL methods can aid in recognizing interlocking structures, a DL model was implemented (described in Methods section). Non-interlocked (unlocked) geometries exhibit obviously ~ 0 elastic stiffness (friction can produce small perturbations of average stress), whereas interlocked structures are able to transmit load via topological interlocking of their constituents, leading to stiffness values much greater than 0, as previous sections have shown. The geometry' stiffness values were mapped into binary values, corresponding to 0 or 1 for unlocked or interlocked structures, respectively, and provided to the DL model for training. As shown in Fig. 1D, really high accuracy is reached by the DL model only for $\sim 20\%$ of training data density, demonstrating that the DL model is able to almost perfectly capture the interlocking mechanism even with only a few thousands of training samples. The sensitivity of accuracy, precision and recall to the training data density is reported in Supporting Information Fig. A.7A, confirming the high performances of the model with small percentages of training data. Note how the ability of the model to recognize actual interlocking structures (i.e., the recall) is almost invariant with the training data density within the tested range ($\sim 99.99\%$ for training data density $\sim 0.5\%$), probably due to the smaller fraction of unlocked structures (1352 out of a total of 19,946 geometries). Despite the simplicity of the structures (i.e., single 2-D interlocking interface), these results prove that DL methods can be used to design materials based on the interlocking mechanism. Indeed, the proposed DL approach could easily be extended to more complex architectures for materials design or study of natural systems, which exploit the interlocking scheme.

3.3. Mechanical properties prediction

To investigate the structure-property relationships in 2-D interlocking interfaces, a DL model was implemented. The predicted mechanical property values of a 10 by 10 system are compared to the FE values (ground truth) in Fig. 3A, in which ideal predictions are represented by the 45°-inclined line (predicted values equal to target values). High coefficients of determination can be reached by the predicted values for each mechanical property, however, decreasing performances from stiffness to toughness prediction are captured from the plots. It is evident how the stiffness is more easily predictable than the other two properties. Analogous conclusions can be drawn by looking at all the considered metrics in Table 1. We attribute such behavior to the high nonlinearity of the problem, which represents a greater source of uncertainty for the FE modeling itself. Specifically, being the toughness values computed as the area underneath the effective stress-strain curve, they are more sensitive to numerical fluctuations in the FE solver solution. In addition, the stress singularities in the elastic region of the base material at the angular corners of the interlocking structures induce an intrinsic approximation in the FE modeling; further improvements towards large-scale smooth structures are left for future works. Nevertheless, relative MAE values (with respect to the target property range) of $\sim 1 - 2\%$ as well as high accuracy levels with values $> 96\%$ for every material property are obtained, as reported in Table 1. As an example (the closest one available), previous pioneering works of Charles Yang et al. (2019, 2020) on prediction of 2-D composite properties beyond the elastic limit using ML methods reached maximum R^2 values ~ 0.91 for strength and much lower values for stiffness and toughness. It must be underlined, however, that their ML models were not optimized for the specific task and limits of the models were not investigated. Instead, our results (Table 1) refer to a DL model obtained by tuning some of its hyperparameters. More in detail, in Supporting Information Fig. A.5, the comparison between the different models in terms of MAE, R^2 and accuracy, highlights how increasing the number of convolutional filters tend to improve the overall performances, at the expense of computational

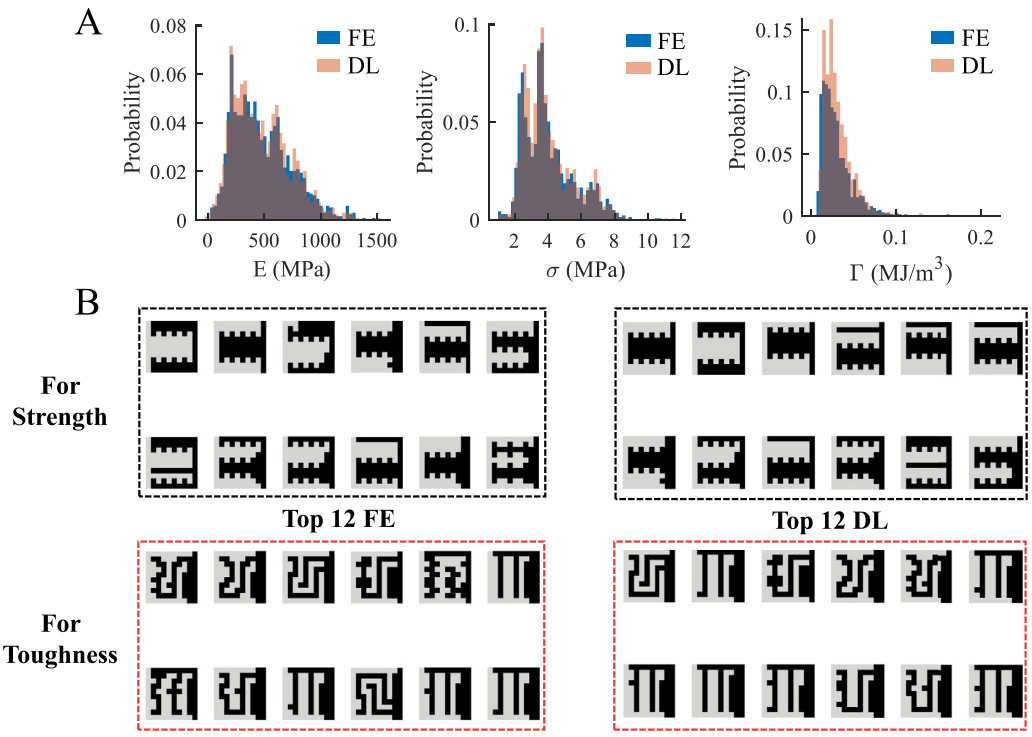

Fig. 4. **(A)** Probability histograms of DL and FE mechanical properties evaluated on test data. DL values are obtained by the tuned DL model with 85:15 training-(validation-test) split in a trial. **(B)** Comparison top 12 high-performing geometries sorted in descending order by column, for each row, from FE simulations and DL model predictions for strength and toughness. Geometries from the 10 by 10 system.

costs. The best two models arising from Fig. A.5 were subsequently selected by doubling their number of filters (Supporting Information Fig. A.6). The optimized architecture consists of three convolutional blocks, with 128 filters and patch size (3,3), and a fully-connected layer with 256 neurons (not further optimized in order to balance the trade-off between accuracy and computational costs). Analogously to the interlocking classification model, the sensitivity of the model performances to the training data density was investigated, as reported in Supporting Information Fig. A.7B. After a training data density of ~ 50%, the metrics values converge to a plateau, demonstrating that with only ~ 9000 training data our DL model is able to accurately solve the structure-property relationship problem. Finally, to have a global statistical picture of the DL model accuracy, a comparison of the probability distributions of FE and DL stiffness, strength and toughness values is displayed in Fig. 4A for test data from the 10 by 10 system. The shape of the histograms for the three mechanical property values predicted by our DL model globally matches that of the target values (FE), covering also the same range of magnitudes.

3.3.1. Patterns learned by the DL model

Opening the "black-box" is crucial to understand which features and patterns does the DL model learn. In Fig. 3C, 9 convolutional filters from the first layer associated to the highest-toughness geometry in the 10 by 10 system are shown. It is clear how the model can recognize some portions of a single phase, assuming uniform values in the resulting image. On the other hand, it seems mainly to be capturing some geometric features, intuitively related to the contact regions between the two phases. Thus, each first-layer filter appears to relate specific contact features to the considered mechanical properties. As deeper layers are considered, the level of abstraction tends to increase. Fig. 3D displays such concept more clearly: after the first convolutional layer, the filters' size is decreased by the average pooling layer, leading to 5×5 pixel representations, which lack of an intuitive human interpretability. Due to the small size (2×2), the third-layer filters are not shown. Despite the difficulty to interpret the learned representations of the last two convolutional blocks, the hyperparameters tuning proved their importance to accurately predict the mechanical properties of interlocking interfaces. Such trade-off between intelligibility of the learning process and accuracy of predictions arises as a great challenge for future work.

To demonstrate the ability of our DL model to relate specific geometric patterns to specific mechanical property ranges, we compare in Fig. 4B the top 12 high-performing interlocked geometries for strength and toughness obtained by the FE and DL model. The ranks performed by the DL predictions do not perfectly match those from the FE modeling, however, our DL model is able to predict the same interlocking patterns for the two classes of structures. Specifically, almost all the high-strength and high-toughness top 12 geometries ranked by the FE model are recognized also by the DL model. Since the best geometries are characterized by small geometric differences (for some cases only one building block changes), they also exhibit close mechanical property values, thus leading to small variations in the DL ranks compared to the FE results. Same conclusions can be drawn by looking at the top 12 high-stiffness geometries, shown in Supporting Information Fig. A.8.

3.4. Predictions on larger design spaces via transfer learning

One of the limitations of our DL approach might be found on the geometry resolution: if the DL model is trained on a small resolution design space, will it be able to predict the interlocking mechanism and the mechanical properties of interlocking structures sampled from larger resolution design spaces ? To answer this question, our DL models were first pre-trained on the 10 by 10 system data set (random 85:15 train-test split), resizing the input images by a factor of 2 i.e., training the models with 20×20 pixel images; thus, the design space was equally scaled along the x- and y-direction. In this way, we took advantage from the fact that the 10 by 10 geometries represent simply a subset of the 20 by 20 system. From the ~ 3000 interlocked and ~ 3000 unlocked geometries, which represent a subset of all the combinations of the 20 by

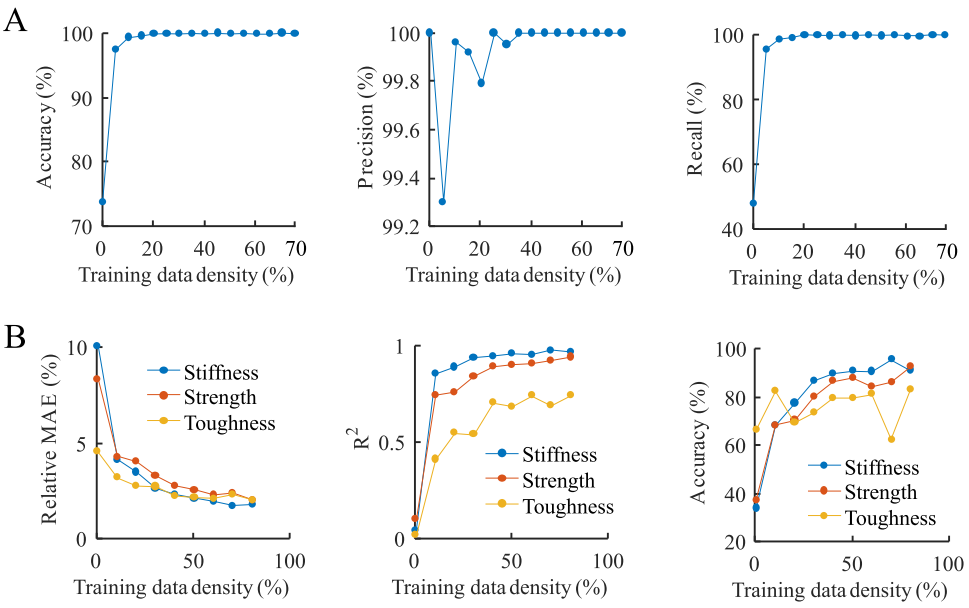

Fig. 5. DL models performances evaluation exploiting of a transfer learning approach i.e., feeding the pre-trained DL models with new data from a larger design space (20 by 20 system in this case). **(A)** Interlocking classification metrics for increasing training data density values from a larger design space. **(B)** Relative MAE, R^2, and accuracy ($k = 0.05$) for mechanical properties prediction evaluated at increasing training data density values from a larger design space. The tuned DL model for properties prediction is adopted for these computations, without loss of generality.

20 system, only a percentage was used to further training the models, whereas the other data were employed as test data to investigate the DL models' ability to generalize from a few new examples. Fig. 5A shows the variation of the metrics relative to interlocking classification, when new training data are provided from larger resolution geometries, at different densities (from 0.05% to 70% with a step of 5%). Accuracy and recall start with low values, however, approach very fast the upper bound, stabilizing at values around 99.98% as the training data density attains values around ~ 20%. Precision seems to be initially not really sensitive to new training data, however, it reaches a plateau at a density of ~ 40%. Similar results are also obtained for the prediction of mechanical properties. The performances of the DL model in terms of relative MAE, R^2, and accuracy ($k = 0.05$) tend to improve as more larger resolution geometries are fed into the network for training. At a training data density of ~ 60%, the performances seem to be attaining constant values, slightly worse than those reported in Table 1. The only unexpected behavior can be observed for the accuracy of the toughness prediction, which basically oscillates around a value of 75%, without an effective improving trend. This may arise from the sensitivity of the toughness values (as the area under the stress-strain curve) to numerical fluctuations in the FE solver, thus leading to a greater unpredictability.

4. Discussion

The results of this work can be globally seen as the proof of the possibility to apply DL methods for the design of 2-D interlocking features. DL approaches may indeed become unavoidable to enlarging the design space. Since complex geometries arise usually from a large number of possible combinations of smaller parts (as in our method we use basic building blocks), typical physics-based modeling approaches, such as FE modeling, tend to loose their attraction due to the required high computational costs. Not only the geometric complexity but also the high nonlinearity of the problem (specifically for material properties prediction) makes DL methods a suitable strategy for the design of interlocking structures (which could be considered just as an example). Our cellular automaton-like method together with DL methods represent thus only one possible way of enlarging the design space of 2-D interlocking structures.

Despite our trivial application of interlocking classification, more complex structures, such as strong plant shells appearing to gain strength and toughness via interlocking features, could be studied using the same approach, without generality restrictions. At the same way, DL models for mechanical properties predictions may be extended to more complex systems or integrated in algorithms for materials inverse design. In addition, our attempts to open the "black-box" and to have models able to learn from just a few examples are in the direction of understanding and leveraging, respectively, the current DL methods to increase their accuracy (reliability) and to decrease their computational costs.

5. Conclusions

In this work, we use for the first time DL methods to study the interlocking mechanism and to predict the mechanical properties of 2-D interlocking features. We show how the design of interlocking interfaces/joints can leverage the powerful abilities of DL methods to (1) unveiling the interlocking mechanism; (2) quickly and accurately predicting material properties in high nonlinear problems, such as contact, plastic behavior, and damage initiation and evolution; and (3) enlarging the design space. Besides, we prove that DL models have "memory" of the previous recognized patterns in smaller design spaces, thus leading to the possibility to exploring larger design spaces (for example, increasing the resolution in our cellular automaton-like method) with relative little extra computational effort. Our work could pave the way for future applications of DL methods to better understanding the peculiar mechanical properties of interdigitated features in biological systems, and design of engineered novel interlocked materials.

Declaration of Competing Interest

The authors declare that they have no known competing financial interests or personal relationships that could have appeared to influence the work reported in this paper.

Supplementary material

Supplementary material associated with this article can be found, in the online version, at doi:10.1016/j.apples.2021.100056

References

Abadi, M., Barham, P., Chen, J., Chen, Z., Davis, A., Dean, J., Devin, M., Ghemawat, S., Irving, G., Isard, M., et al., 2016. Tensorflow: a system for large-scale machine learning. In: 12th {USENIX} Symposium on Operating Systems Design and Implementation ({OSDI} 16), pp. 265–283.

Alpaydin, E., 2020. Introduction to Machine Learning. MIT Press.
Bajaj, D., Park, S., Quinn, G.D., Arola, D., 2010. Fracture processes and mechanisms of crack growth resistance in human enamel. JOM 62 (7), 76–82.
Barthelat, F., Tang, H., Zavattieri, P., Li, C.-M., Espinosa, H.D., 2007. On the mechanics of mother-of-pearl: a key feature in the material hierarchical structure. J. Mech. Phys. Solids 55 (2), 306–337.
Barthelat, F., Yin, Z., Buehler, M.J., 2016. Structure and mechanics of interfaces in biological materials. Nat. Rev. Mater. 1 (4), 1–16.
Beygelzimer, Y., Kulagin, R., Fratzl, P., Estrin, Y., 2021. The earth's lithosphere inspires materials design. Adv. Mater. 33 (3), 2005473.
Bock, F.E., Aydin, R.C., Cyron, C.J., Huber, N., Kalidindi, S.R., Klusemann, B., 2019. A review of the application of machine learning and data mining approaches in continuum materials mechanics. Front. Mater. 6, 110.
Chen, C.-T., Gu, G.X., 2020. Generative deep neural networks for inverse materials design using backpropagation and active learning. Adv. Sci. 7 (5), 1902607.
Chen, I.H., Yang, W., Meyers, M.A., 2015. Leatherback sea turtle shell: a tough and flexible biological design. Acta Biomater. 28, 2–12. doi:10.1016/j.actbio.2015.09.023.
Gao, C., Hasseldine, B.P., Li, L., Weaver, J.C., Li, Y., 2018. Amplifying strength, toughness, and auxeticity via wavy sutural tessellation in plant seedcoats. Adv. Mater. 30 (36), 1800579.
Gao, C., Li, Y., 2019. Mechanical model of bio-inspired composites with sutural tessellation. J. Mech. Phys. Solids 122, 190–204.
Gu, G.X., Chen, C.-T., Buehler, M.J., 2018. De novo composite design based on machine learning algorithm. Extreme Mech. Lett. 18, 19–28.
Gu, G.X., Chen, C.-T., Richmond, D.J., Buehler, M.J., 2018. Bioinspired hierarchical composite design using machine learning: simulation, additive manufacturing, and experiment. Mater. Horiz. 5 (5), 939–945.
Hornik, K., 1991. Approximation capabilities of multilayer feedforward networks. Neural Netw. 4 (2), 251–257.
Jaslow, C.R., 1990. Mechanical properties of cranial sutures. J. Biomech. 23 (4), 313–321.
Kauderer-Abrams, E., 2017. Quantifying translation-invariance in convolutional neural networks. arXiv preprint arXiv:1801.01450.
Khoshhesab, M.M., Li, Y., 2018. Mechanical behavior of 3D printed biomimetic koch fractal contact and interlocking. Extreme Mech. Lett. 24, 58–65.
Koester, K.J., Ager, J., Ritchie, R., 2008. The true toughness of human cortical bone measured with realistically short cracks. Nat. Mater. 7 (8), 672–677.
Krauss, S., Monsonego-Ornan, E., Zelzer, E., Fratzl, P., Shahar, R., 2009. Mechanical function of a complex three-dimensional suture joining the bony elements in the shell of the red-eared slider turtle. Adv. Mater. 21 (4), 407–412.
LeCun, Y., Bengio, Y., Hinton, G., 2015. Deep learning. Nature 521 (7553), 436–444.
Lee, N., Horstemeyer, M., Rhee, H., Nabors, B., Liao, J., Williams, L.N., 2014. Hierarchical multiscale structure–property relationships of the red-bellied woodpecker (*Melanerpes carolinus*) beak. J. R. Soc. Interface 11 (96), 20140274.
Li, Y., Ortiz, C., Boyce, M.C., 2011. Stiffness and strength of suture joints in nature. Phys. Rev. E 84 (6), 062904.
Li, Y., Ortiz, C., Boyce, M.C., 2012. Bioinspired, mechanical, deterministic fractal model for hierarchical suture joints. Phys. Rev. E 85 (3), 031901.
Li, Y., Ortiz, C., Boyce, M.C., 2013. A generalized mechanical model for suture interfaces of arbitrary geometry. J. Mech. Phys. Solids 61 (4), 1144–1167.
Lin, E., Li, Y., Ortiz, C., Boyce, M.C., 2014. 3D printed, bio-inspired prototypes and analytical models for structured suture interfaces with geometrically-tuned deformation and failure behavior. J. Mech. Phys. Solids 73, 166–182.
Lin, H., Jegelka, S., 2018. ResNet with one-neuron hidden layers is a universal approximator. Adv. Neural Inf. Process. Syst. 31, 6169–6178.
Liu, Z., Zhang, Z., Ritchie, R.O., 2020. Interfacial toughening effect of suture structures. Acta Biomater. 102, 75–82.
Malik, I.A., Barthelat, F., 2018. Bioinspired sutured materials for strength and toughness: pullout mechanisms and geometric enrichments. Int. J. Solids Struct. 138, 118–133.
Malik, I.A., Mirkhalaf, M., Barthelat, F., 2017. Bio-inspired "jigsaw"-like interlocking sutures: modeling, optimization, 3D printing and testing. J. Mech. Phys. Solids 102, 224–238.
Mirkhalaf, M., Barthelat, F., 2017. Design, 3D printing and testing of architectured materials with bistable interlocks. Extreme Mech. Lett. 11, 1–7.
Mirkhalaf, M., Tanguay, J., Barthelat, F., 2016. Carving 3D architectures within glass: exploring new strategies to transform the mechanics and performance of materials. Extreme Mech. Lett. 7, 104–113.
Mirkhalaf, M., Zhou, T., Barthelat, F., 2018. Simultaneous improvements of strength and toughness in topologically interlocked ceramics. Proc. Natl. Acad. Sci. 115 (37), 9128–9133.
Miura, T., Perlyn, C.A., Kinboshi, M., Ogihara, N., Kobayashi-Miura, M., Morriss-Kay, G.M., Shiota, K., 2009. Mechanism of skull suture maintenance and interdigitation. J. Anat. 215 (6), 642–655.
Ortiz, C., Boyce, M.C., 2008. Bioinspired structural materials. Science 319 (5866), 1053–1054.
Rivera, J., Hosseini, M.S., Restrepo, D., Murata, S., Vasile, D., Parkinson, D.Y., Barnard, H.S., Arakaki, A., Zavattieri, P., Kisailus, D., 2020. Toughening mechanisms of the elytra of the diabolical ironclad beetle. Nature 586 (7830), 543–548.
Sapala, A., Runions, A., Routier-Kierzkowska, A.-L., Gupta, M.D., Hong, L., Hofhuis, H., Verger, S., Mosca, G., Li, C.-B., Hay, A., et al., 2018. Why plants make puzzle cells, and how their shape emerges. Elife 7, e32794.
Senior, A.W., Evans, R., Jumper, J., Kirkpatrick, J., Sifre, L., Green, T., Qin, C., Žídek, A., Nelson, A.W., Bridgland, A., et al., 2020. Improved protein structure prediction using potentials from deep learning. Nature 577 (7792), 706–710.
Wang, W., Sun, Y., Lu, Y., Wang, J., Cao, Y., Zhang, C., 2020. Tensile behavior of bio-inspired hierarchical suture joint with uniform fractal interlocking design. J. Mech. Behav. Biomed. Mater. 113, 104137.
Wegst, U., Ashby, M., 2004. The mechanical efficiency of natural materials. Philos. Mag. 84 (21), 2167–2186.
Wegst, U.G., Bai, H., Saiz, E., Tomsia, A.P., Ritchie, R.O., 2015. Bioinspired structural materials. Nat. Mater. 14 (1), 23–36.
Yang, C., Kim, Y., Ryu, S., Gu, G.X., 2019. Using convolutional neural networks to predict composite properties beyond the elastic limit. MRS Commun. 9 (2), 609–617.
Yang, C., Kim, Y., Ryu, S., Gu, G.X., 2020. Prediction of composite microstructure stress-strain curves using convolutional neural networks. Mater. Des. 189, 108509.
Yang, Z., Yabansu, Y.C., Al-Bahrani, R., Liao, W.-k., Choudhary, A.N., Kalidindi, S.R., Agrawal, A., 2018. Deep learning approaches for mining structure-property linkages in high contrast composites from simulation datasets. Comput. Mater. Sci 151, 278–287.
Zhavoronkov, A., Ivanenkov, Y.A., Aliper, A., Veselov, M.S., Aladinskiy, V.A., Aladinskaya, A.V., Terentiev, V.A., Polykovskiy, D.A., Kuznetsov, M.D., Asadulaev, A., et al., 2019. Deep learning enables rapid identification of potent DDR1 kinase inhibitors. Nat. Biotechnol. 37 (9), 1038–1040.